Published in Journal of Applied Physics 111, issue 12, 124906-124913, 2012
which should be used for any reference to this work


# Laser-pumped paraffin-coated cell rubidium frequency standard

Thejesh Bandi,[a] Christoph Affolderbach, and Gaetano Mileti
*Laboratoire Temps-Fréquence (LTF), Institut de Physique, Université de Neuchâtel, Avenue de Bellevaux 51, 2000 - Neuchâtel, Switzerland*

We have realized and studied a rubidium atomic frequency standard based on a paraffin-coated cell, exhibiting a short-term frequency stability $<3\times10^{-12}\ \tau^{-1/2}$ between $\tau=1$ and 100 s. Characterization of the wall-coating is performed by measuring the $T_1$ and $T_2$ relaxation times. Perturbations of the medium- to long-term clock stability, due to variations in the laser-intensity, laser frequency, the microwave power shift, and the shifts due to temperature variations are measured and analyzed. A method for reducing the intensity light-shift by detuning the laser frequency and the resulting improvement in clock stability is demonstrated. This work is of relevance for further improvements on Rb cell standards using anti-relaxation wall-coating technology.

## I. INTRODUCTION

Compact atomic frequency standards exploit a ground-state microwave transition (e.g., in Rb) to provide the stable atomic frequency reference to which the frequency of a quartz oscillator is stabilized. At the heart of a conventional rubidium atomic frequency standard, for example, the ones used in global positioning system (GPS),[1] atomic rubidium contained in glass-cells also filled with buffer gases is used. Buffer gases help to prevent the polarized Rb atoms from colliding on to the cell walls and to obtain narrow resonance lines by reducing the mean free path of a Rb atom to less than the microwave photon's wavelength of few cm (Dicke narrowing[2,3]). Such narrow linewidths and a high resonance amplitude are essential for a good short-term stability of the clock. Alternative to the above approach, an evacuated glass cell whose inner walls are coated with an anti-relaxation material and filled with Rb vapor could be adopted as a new heart[4–6] for the clocks. The first studies on collisions between alkali atoms and coatings, such as paraffins ($C_nH_{2n+2}$) or silanes (e.g., dimethyldichlorosilane) were done by Bouchiat and Brossel during 1960s[7] by adopting Franzen's method of *relaxation in the dark*.[8] They used a paraffin coated cell and found that the alkali atoms undergo about $10^4$ collisions before they lose their state of polarization. Franzen's technique of relaxation in the dark was used by Liberman *et al.* for studying the relaxation of caesium atoms in paraffin wall-coated cells,[9] whereas a variant of this technique was adopted by Graf *et al.*[10] in their studies. Although the idea to use wall-coated cells in an atomic frequency standard was suggested by Robinson *et al.*[4] in the late 1950s, it was not realized due to the limitations in operating temperatures of such cells (incompatible with the use of lamps for optical pumping) and other technological difficulties, such as control of the coating quality. Part of these drawbacks has been overcome with laser optical pumping; however, a reliable commercial product is yet to be realized. Recently, the interest in wall-coated cells for high-precision spectroscopy and metrology is growing again, because coated cells represent good candidates to realize high-performance or micro-fabricated devices, such as miniaturized atomic clocks and/or atomic magnetometers.[11,12]

The double-resonance (DR) spectroscopy requires two electro-magnetic fields: an optical field to polarize the atoms by optical pumping, and a microwave field to drive the ground-state hyperfine clock transition that serves as an atomic frequency reference.[1] A polarized atom in an uncoated, evacuated glass-cell without buffer-gas can depolarize by only one collision on the wall and hence the achievable DR-linewidth is several tens of kHz for a cm-scale cell, which corresponds to a clock short-term stability of approximately $1\times10^{-9}$ at 1 s. This assumes that the DR signal is not further degraded due to time-of-flight (TOF) effect (broadening due to the limited interaction time of an atom in the laser beam path). In contrast, a cell whose inner walls are coated with a high-quality anti-relaxation material preserves the polarized state of an alkali atom for more than a few hundred to few thousand collisions, depending on the size of the cell. The long-lived atomic polarization in turn increases the Q-factor of the atomic resonance line and thereby contributes to improve the short-term stability of the clock. Typical spin-relaxation times in wall-coated cells can be as large as $\approx$1 s, and narrow line-widths of the clock transition around 200 Hz or even as low as 10 Hz were observed.[5] In contrast to the above mentioned work on alkanes (conventional paraffins), the recent work of Balabas *et al.*[13] shows that it is possible for the atomic polarization life-times to exceed 1 min, with atoms undergoing up to $10^6$ collisions with an alkene-based coating. Basic studies on the application of wall-coated cells for Rb frequency standards are reported in Refs. 14–18.

Here, we present our studies on a laser-pumped, microwave-optical double-resonance rubidium standard using atomic $^{87}$Rb in a paraffin-coated cell. The cell used here has smaller dimensions than the previously studied ones,[5,15] in view of a compact, high-performance Rb standard. In Sec. II, the wall-coated cell is characterized by measuring the Rb ground-state relaxation times. The clock experimental setup is explained in Sec. III, along with the DR signal properties. In

[a]thejesh.bandi@unine.ch.

Sec. IV, we report the systematic shifts, $\Delta\nu$, of the $^{87}$Rb $5^2S_{1/2}|F_g = 1, m_F = 0\rangle \rightarrow |F_g = 2, m_F = 0\rangle$ *clock transition*, from the unperturbed hyperfine ground-state frequency of $\nu_{Rb} = 6834682610.90429(9)$ Hz,[19] such as intensity and frequency light shifts,[20,21] microwave power shift[22,23] and temperature shifts.[24] The influence of these parameters on the clock frequency instability is also evaluated. In Sec. V, the clock stability (Allan deviation) is measured and compared to the short-term stability analysis. Finally, the limitations on the clock stability on medium to long-term time-scales are identified and discussed in view of required future improvements.

## II. CHARACTERIZATION OF THE WALL-COATING

A paraffin-coated ($C_{40}H_{82}$) cell shown in Fig. 1(a) with an inner volume of ~1.4 cm$^3$ was used in our measurements. The cell has two distinctive regions; a cell-volume, which holds the vapor of interrogated Rb atoms, and the cell-stem that acts as a reservoir for metallic Rb.

A laser source emitting at the Rb D2-line (780 nm) optically pumps the atoms from the $^{87}$Rb, $F_g = 2$ hyperfine state as shown in Fig. 1(b) (using a linear light polarization). The excited state ($F_e$) manifold is not resolved due to Doppler broadening; however, the strongest contribution to the pumping process mainly comes via the $F_e = 2$ state. The laser beam passes through an acousto optical modulator (AOM), which was used as an optical switch as shown in Fig. 1(c). The optical pumping time and also the dark time were varied using the *on* and *off* time durations of the AOM rf-drive. During the dark time, $\tau_d$, the atoms undergo relaxation mainly because of random electronic depolarization by collisions with the walls,[25] and also due to reservoir effect.[26]

The absorption signals of the laser passing through the wall-coated cell were recorded as a function of the dark time using the photodetector. This gives a measure of the number of atoms, N2, in the $F_g = 2$ state at the end of the dark time, as a function of $\tau_d$, and eventually reaching a saturation termed as $N2_{eq}$ in Fig. 2. The longitudinal relaxation time, $T_1$, is extracted by a single exponential fit function given by Ref. 25,

$$N2(\tau_d) = N_0 + N2_{eq}(1 - e^{-\tau_d/T_1}), \qquad (1)$$

where $\tau_d$ is the dark time, $N_0$ is measured to be zero within the experimental errors, and $N2_{eq}$ is normalized to 1 (arb. unit). The fitted value of $T_1 = 25.1(0.6)$ ms (at T = 300 K) gives an estimate of about 2255 wall collisions before an atom loses its polarized state. To the first-order approximation, we calculate the number of wall collisions, $N = \mathrm{T}_1 \frac{A}{V}\sqrt{\frac{8k_BT}{\pi M}}$, where $k_B$ is the Boltzmann constant, $M$ is the mass of $^{87}$Rb atom, and $\frac{V}{A} = \frac{R}{2(1+R/L)}$ is the ratio of volume to area of the cell considering the cylindrical geometry, where $R$ and $L$ are the internal radius and length of the cell, respectively.[27] Here, the $T_1$ relaxation time is measured for the total hyperfine ground state, which includes the contribution from all the Zeeman levels.

The coherence between two states, measured by the transversal relaxation time, $T_2$, is also an influencing parameter for the clock short-term stability. Here, the $T_2$ relaxation time is measured only for *the clock transition*, by the double-resonance mechanism (explained in Sec. III). Extrapolation of the clock transition linewidth (FWHM) to zero pump-light intensity allows one to extract $T_2$ using the relation, FWHM $= 1/\pi T_2$, when other sources of line broadening are negligible.[28] A relaxation time of coherences, $T_2 = 0.9$ ms is obtained from the line-fit as shown in Fig. 3.

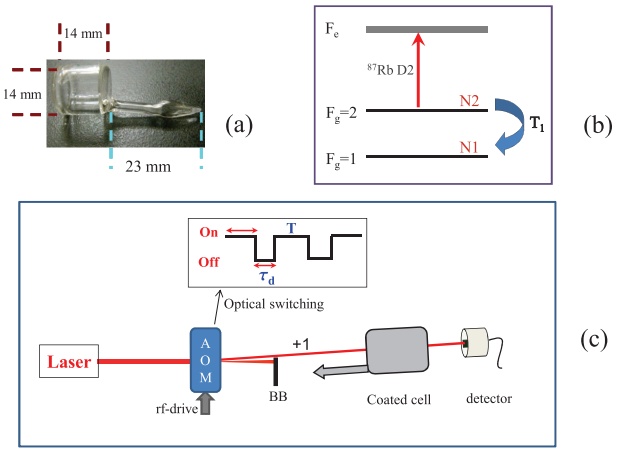


FIG. 1. (a) Paraffin-coated cell with a reservoir stem on its right-hand side, (b) conceptual diagram of relaxation of population in the ground-state hyperfine components, and (c) the schematic setup for measuring the $T_1$ by relaxation in the dark method, BB: beam blocker. The inset shows the optical switching time.

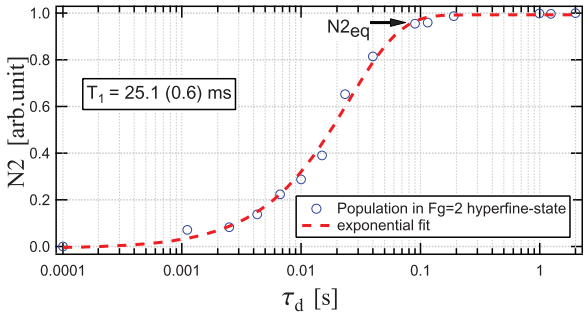


FIG. 2. The experimental $T_1$ extracted by the exponential fit (Eq. (1)).

## III. CLOCK EXPERIMENTAL SETUP AND DR SPECTROSCOPY

The schematic of our microwave-optical double-resonance experimental clock setup is shown in Fig. 4. A distributed-feedback (DFB) laser source emitting on the D2 transition at 780 nm optically pumps the $^{87}$Rb atoms.[29] A narrow beam of 1.9 mm diameter was used for optical pumping; as an atom moves freely and quickly enough to sample a large fraction of cell volume, expansion of the optical beam to fill the entire cell was not required.[30] A first feed-back loop is used for laser frequency stabilization: the signal from a saturated-absorption spectroscopy setup with a separate evacuated Rb cell is used to stabilize the laser frequency to a selected sub-Doppler transition. For a part of the experiments explained in Sec. IV A 1, an optional AOM is used for detuning the laser beam before stabilizing to the reference cell. The

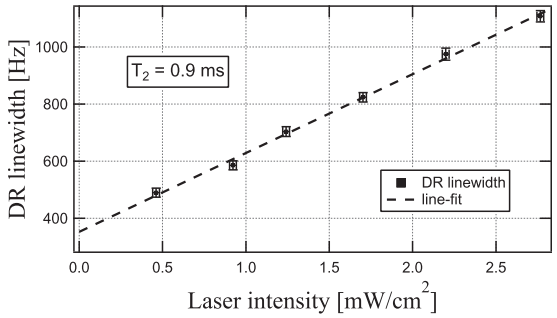


FIG. 3. The DR linewidth as a function of laser intensity for determination of coherence relaxation time, $T_2$.

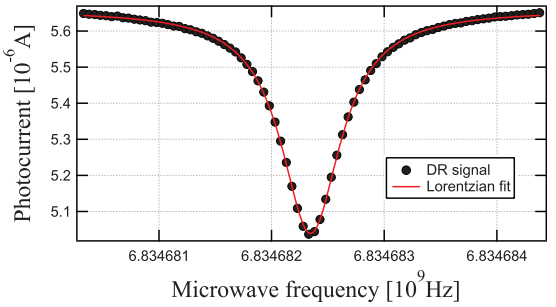


FIG. 5. Double-resonance signal with a linewidth of 642 Hz and a contrast of 11%.

clock physics package (PP) holds the wall-coated cell at its heart. The temperatures of cell volume ($T_v$) and stem ($T_s$) are maintained at a small gradient to avoid the formation of Rb droplets on the coated walls of the cell volume ($T_s < T_v$). The cell is placed inside a small $TE_{011}$ magnetron cavity,[22] which is tuned to resonate at the $^{87}$Rb ground state frequency of 6.835 GHz, and has a Q-factor of ∼341. A dc magnetic field of 40 mG is applied in the direction of the laser propagation using coils that are wound around the cavity. This field splits the degenerate ground-state hyperfine levels into their Zeeman sub-levels, of which only the $m_F = 0 \leftrightarrow 0$ *clock transition* is of interest here. This assembly is surrounded by two $\mu$–metal magnetic shields with a measured longitudinal shielding factor of 3067. A second feed-back loop is used to stabilize the microwave frequency from a synthesizer (or local oscillator, LO) to the $^{87}$Rb microwave clock transition. Once the clock loop is established, the 10 MHz output from the LO is compared with that of the 10 MHz signal from an active hydrogen maser using a frequency comparator. Finally, the clock frequency is recorded using a computer interface.

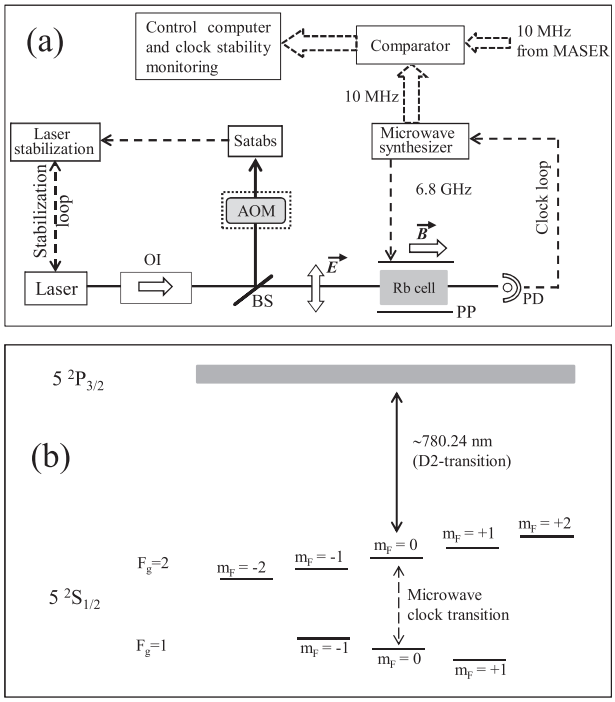


FIG. 4. (a) Schematic of the clock experimental setup. Solid line shows the laser beam and the dashed lines represent the electrical connections. The AOM shown inside a dotted box is optional to reduce the intensity light-shift. BS: beam splitter, PD: photodetector, OI: optical isolator, and PP: physics package. The laser electric field, $\vec{E}$ and the dc magnetic field, $\vec{B}$ directions are indicated. (b) $^{87}$Rb-D2 transition hyperfine structure, with Zeeman splittings between the ground state hyperfine energy levels in the presence of a static magnetic field. Allowed microwave transitions are $\Delta m_F = 0, \pm 1$.

### A. Double resonance signals

DR spectroscopy involves two resonant electromagnetic fields. First, the optical pumping resonant field (Rb D2-line, $5^2S_{1/2} \rightarrow 5^2P_{3/2}$) emitted by the laser source to creates a ground-state polarization by pumping the atoms to one of the atomic ground states. The second resonant field interrogates at microwave frequency to drive the ground-state hyperfine clock transition around 6.835 GHz. In our DR experiments, the laser was locked to the $5^2S_{1/2}F_g = 2 \rightarrow 5^2P_{3/2}F_e = 3$ direct transition on the $^{87}$Rb D2-line, with an optical intensity of about 11 $\mu$W/cm$^2$ incident on the clock cell. The cell and stem temperatures were regulated at $T_v = 329$ K and $T_s = 321$ K, respectively. A microwave power of 1 $\mu$W was injected into the cavity. The DR signal in these conditions is shown in Fig. 5. It has a narrow linewidth of 642 Hz with an amplitude and contrast of 0.62 $\mu$A and 11%, respectively. The center frequency is $\nu_{DR} = 6.8346823$ GHz here. In our DR signals, we do not observe any Doppler-broadened pedestal that would be expected when using a travelling microwave field due to the phase variations over the cell volume.[5,14] In contrast to the use of typical cylindrical cavities having $TE_{011}$ mode[15] (where the cell volume occupies different microwave phase regions), in our magnetron cavity the cell only occupies regions of same microwave phase; therefore, the broad pedestal is suppressed.

## IV. SYSTEMATIC CLOCK FREQUENCY SHIFTS

Though first-order shifts due to magnetic field variations are absent on the clock transition frequency, the other parameters, such as, variations in laser intensity and frequency, the power fluctuations of microwave, and the residual temperature fluctuations can induce shifts on the clock transition and degrade the clock stability on medium- to long-term time scales. Therefore, control or suppression of the influence of these effects is needed for improving the clock performance. We perform quantitative measurements of AC Stark shift (also referred to as intensity or frequency light-shift (LS)), microwave power shift, and temperature shifts due to the

cell's volume and stem. The influence of these perturbations on the clock instability is evaluated.

### A. Light-shift (AC Stark shift)

The LS[20] of an electromagnetic field on the clock transition is usually encountered in Rb clocks when in continuous wave (CW) operation. This occurs by the light field initiating virtual transitions in the atoms, and in this sense is fundamentally related to the Lamb shift, which arises due to atom's interaction with the vacuum field.[1] The LS, $\Delta\nu_{LS}$, can be written as,[21]

$$\Delta\nu_{LS} \propto \frac{I_L(\nu_L - \nu_{opt})}{(\nu_L - \nu_{opt})^2 + \Gamma^2}, \tag{2}$$

where $\nu_L$ is the laser frequency, $\Gamma$ is the width of the approximately Lorentzian optical absorption centered at the optical atomic transition frequency $\nu_{opt}$, and $I_L$ is the intensity of the light.

#### 1. Intensity light shift ($\alpha$) and its reduction by laser detuning method

From Eq. (2), the intensity LS coefficient, $\alpha$, can be derived as $\alpha = \frac{\delta\nu_{LS}}{\delta I_L}$ at a fixed laser frequency. Experimentally, we determine $\alpha$ by measuring the clock frequency as a function of laser intensity, for the laser frequency stabilized to three different sub-Doppler transitions on the $^{87}$Rb D2-line pumped from $F_g = 2$ to excited states in $5P_{3/2}$ (Ref. 19) as shown in Fig. 6(a). The fitted slopes give the intensity LS coefficients $\alpha$ for the particular laser frequency. The lowest value, obtained

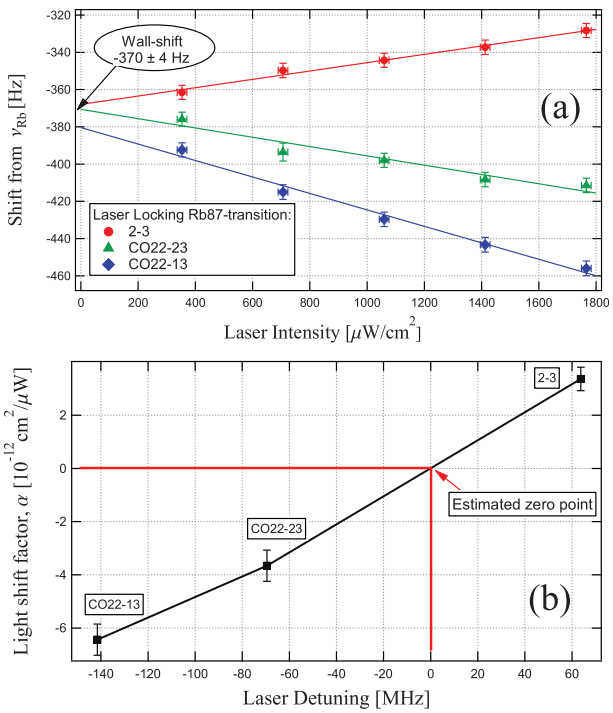


FIG. 6. (a) $^{87}$Rb frequency shift as a function of the interrogating laser intensity. Slopes give the intensity LS coefficient, $\alpha$, (b) dependence of $\alpha$ on laser frequency detuning is shown with reference to the locked transitions using an evacuated Rb cell. The labeling of the $^{87}$Rb transitions correspond as follows; 2-3: $F_g = 2 \rightarrow F_e = 3$, CO22-23: $F_g = 2 \rightarrow F_e = 2,3$ cross-over, and CO22-13: $F_g = 2 \rightarrow F_e = 1,3$ cross-over.

for $F_g = 2 \rightarrow F_e = 3$ direct transition, is $\alpha = +23(3)$ mHz cm$^2/\mu$W. Extrapolation to zero laser intensity gives the value of the clock frequency shift, $\Delta\nu = \nu_{DR} - \nu_{Rb}$, corrected for LS effects, and which is mainly determined by the wall-coating (see Sec. IV C), in this case, it is $\Delta\nu = -370(4)$ Hz. This wall shift depends on the cell temperature, and can vary for different coating material. Also, this shift can change over time depending on the modifications in the coating material.

The dependence of the intensity LS coefficient, $\alpha$, on the laser frequency is shown in Fig. 6(b). One can reduce the effect of intensity LS by detuning the laser frequency, $\nu_L$ closer to $\nu_{opt}$, where $\alpha$ is small.[21] In our experiment, we adopt an AOM for detuning the laser frequency by $-131$ MHz before stabilizing the frequency-shifted beam to the $F_g = 2 \rightarrow F_e = 1,3$ cross-over resonance. Using the unshifted laser frequency for the clock (i.e., detuned by $+131$ MHz with respect to $F_g = 2 \rightarrow F_e = 1,3$ cross-over), a reduced coefficient $\alpha_{redu} = -0.57(4)$ mHz cm$^2/\mu$W was measured, which is a reduction in $\alpha$ by a factor of 40.

*a. Influence on clock instability.* Though the intensity LS influences the clock instability at all integration times, main limitations result on the medium- to long-term time scales. Hence, we estimate the LS contribution to clock instability at $10^4$ s. When the laser frequency is stabilized to the $F_g = 2 \rightarrow F_e = 3$ direct transition, the intensity LS is measured to be $|\alpha| = 23(3)$ mHz cm$^2/\mu$W (cf. Fig. 6(a)). The intensity LS contribution on the clock frequency can be estimated by,

$$\sigma_\alpha = \frac{|\alpha|.\sigma_{I_L}.I_L}{\nu_{Rb}}, \tag{3}$$

where the relative stability of the laser intensity in terms of Allan standard deviation at $10^4$ s is measured to be $\sigma_{I_L} = 5 \times 10^{-3}$. At the operating laser intensity, $I_L = 1059$ $\mu$W/cm$^2$ (chosen for optimized short-term clock stability, see Sec. V), the contribution to the clock instability, $\sigma_\alpha$ is estimated as $1.8 \times 10^{-11}$ at $10^4$ s. Using the AOM for reduction of the intensity LS results in a stability limit of $4.5 \times 10^{-13}$.

#### 2. Frequency light-shift ($\beta$) and dependence on laser intensity

From Eq. (2), when the intensity of the light is kept constant, the frequency LS coefficient is written as $\beta = \frac{\delta\nu_{LS}}{\delta\nu_L}$. Frequency LS can be nullified, e.g., in pulsed mode.[31] In the continuous-wave operation discussed here, this is not possible, but we can reduce $\beta$ by operating at low light intensities.[32] At different fixed light intensities, the value of $\beta$ is evaluated as the slope of the line-fits shown in Fig. 7(a). The zoom-inset at the zero laser detuning frequency shows the measure of the clock frequency shift, $\Delta\nu \approx -372 \pm 4$ Hz, when unperturbed by LS. Dependence of the frequency LS coefficient $\beta$ as a function of pump-light intensity is shown in Fig. 7(b) and is linear in $I_L$, as expected from Eq. (2).

*a. Influence on clock instability.* We estimate the influence of the frequency LS on the clock's instability at $10^4$ s.

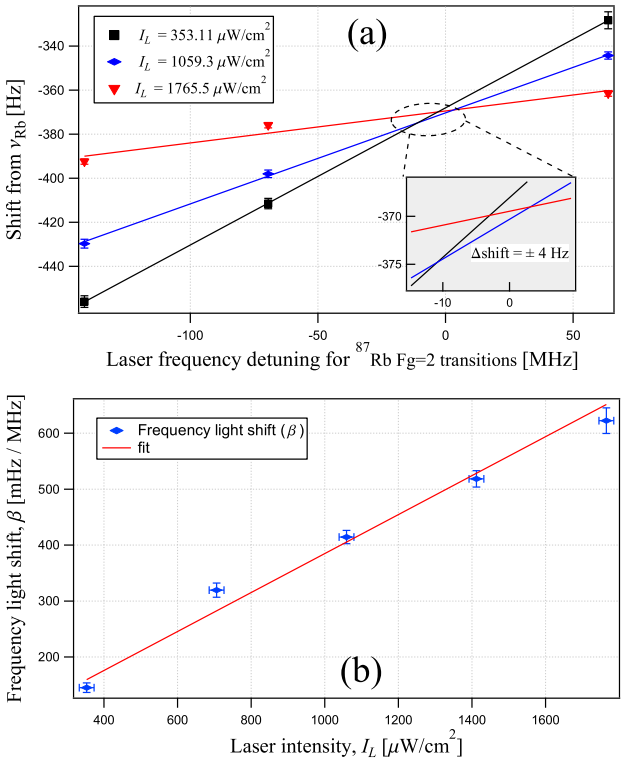


FIG. 7. (a) Clock frequency shifts as a function of the laser frequency detuning; the slopes give the frequency LS, $\beta$, and (b) the dependence of $\beta$ on laser intensity, $I_L$.

At a light intensity of 1059 $\mu$W/cm$^2$, the value of $\beta = 413.8(4)$ mHz/MHz. The stability of the laser frequency, $\sigma_{LF}$, at $10^4$ s measured by beat note method[29] is $<5 \times 10^{-12}$ and $\nu_L = 384.23$ THz. Similar to Eq. (3), we find a contribution of frequency LS to the clock instability as $\sigma_\beta = 1.2 \times 10^{-13}$ at $10^4$ s (also see Table I).

### B. Microwave power shift and influence on clock instability

The microwave power shift of the clock frequency was measured as a function of microwave power (see Fig. 8), with the laser stabilized to $F_g = 2 \rightarrow F_e = 3$ direct transition. A linear-fit gives a shift rate or power-shift coefficient, $\delta_\mu = 3.4(2)$ Hz/dBm ($\simeq 7.8(4)$ Hz/$\mu$W at $P_\mu = 1\,\mu$W). This shift is not negligible, thus requiring a good power stability of the microwave synthesizer. The power stability of our synthesizer is measured to be $\sigma_p = 1 \times 10^{-4}$ at $10^4$ s. With an input power of $P_\mu = 1\,\mu$W, the instability contribution on the clock at $10^4$ s is estimated to be $\sigma_\mu = 1.1 \times 10^{-13}$ (see also Table I). We note that the work of Risely *et al.*[23] shows that the use of wall-coated cells reduces the microwave power shift to $\leq 0.2$ Hz/dBm, which is not observed here.

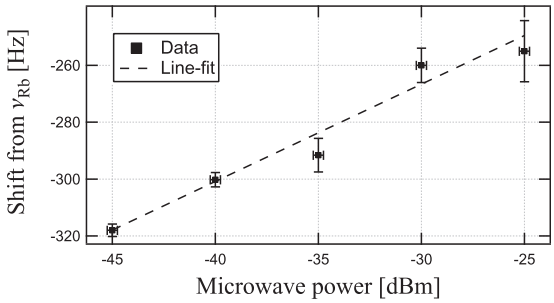


FIG. 8. Frequency shift as a function of microwave power.

### C. Temperature coefficients

The temperature coefficient (TC) of a wall-coated cell is an intrinsic property of the coating material,[24] where the variations in temperature determine the interaction of atoms with the wall-coating and its impact on their polarization state. The TC experiments were performed below the paraffin melting point ($\sim$353 K).[33] Dependence of the clock frequency shift on $T_v$ is shown in Fig. 9(a), its linear-fit slope gives the cell-volume temperature coefficient, $TC_v = +1.39(5)$ Hz/K $\approx 2 \times 10^{-10}$/K. This behavior is related to the adsorption process of the alkali atoms on the coated walls. Assuming a uniform (or average) adsorption energy, $E_a$, in the overall cell volume, the adsorption time, $\tau_a$, of an atom on the walls can be calculated by a simple formula,[14,26,33,34]

$$\tau_a = \tau_0 . e^{\frac{E_a}{k_B T}}, \tag{4}$$

where $\tau_0$ is the period of vibration of the adsorbed atom in the wall potential, $k_B$ is the Boltzmann constant, and $T$ is the absolute temperature. If the temperature increases, Rb atoms spend less time on the wall, which results in a smaller frequency shift and broadening, and vice versa. The wall-shift, $\Delta\nu$, of the clock frequency due to the coating, associated with the temperature and geometry of the cell can be written according to Rahman and Robinson[33] as,

$$\Delta\nu = (\Delta\nu_a)\frac{\tau_a}{\tau_c}, \tag{5}$$

TABLE I. Summary of instability contributions of physical perturbations on the clock transition in medium to long-term time scales.

| Physical effect | Coefficient | Parameter variation at $10^4$ s | Clock instability at $10^4$ s |
|---|---|---|---|
| Intensity light-shift, $\lvert\alpha\rvert$ | 23(3) mHz cm$^2$/$\mu$W | 5.3 $\mu$W/cm$^2$ | $1.8 \times 10^{-11}$ |
| Reduced intensity LS, $\lvert\alpha_{redu}\rvert$ | 0.57(4) mHz cm$^2$/$\mu$W | 5.3 $\mu$W/cm$^2$ | $4.5 \times 10^{-13}$ |
| Frequency light-shift, $\lvert\beta\rvert$ | 413.8(4) mHz/MHz | $<$1.93 kHz | $1.2 \times 10^{-13}$ |
| Cell volume TC | 1.39(5) Hz/K | 10 mK | $2 \times 10^{-12}$ |
| Stem TC | 0.22(3) Hz/K | 10 mK | $3.2 \times 10^{-13}$ |
| Microwave PS | 7.8(4) Hz/$\mu$W | $1 \times 10^{-4}$ $\mu$W | $1.1 \times 10^{-13}$ |

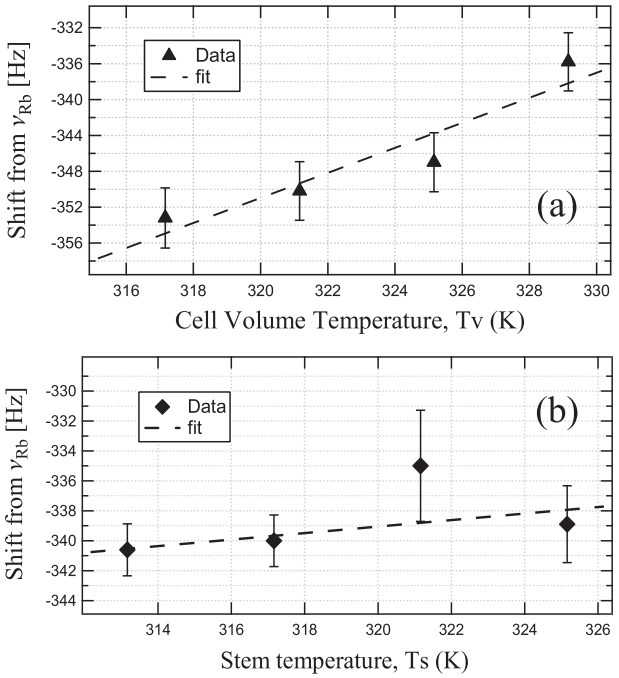


FIG. 9. (a) Clock frequency shift from $\nu_{Rb}$ as a function of cell volume temperature, $T_v$, when $T_s$ is kept constant at 313 K. The closed triangles depict the measured data and the dashed line shows the fit to the data with a cell volume temperature coefficient of $TC_v = +1.39(5)$ Hz/K, and (b) clock frequency shift from unperturbed level as a function of stem temperature, $T_s$, when $T_v$ is kept constant at 329 K. Closed diamonds show the experimental data and the dashed line is a linear fit, with a stem temperature coefficient of $TC_s = +0.22(3)$ Hz/K. The laser intensity and microwave power were kept constant during both the measurements of the temperature coefficients.

where $\Delta\nu_a$ is the difference between the resonant hyperfine frequency while the Rb is absorbed on the surface and that in free space, and $\tau_c$ is the correlation time for atom-wall collisions. Considering a spherical geometry, $\tau_c$ depends on the cell radius, $R$, and the mean velocity, $\langle v\rangle$, of the Rb atoms inside the cell and can be written as $\tau_c = 4R/3\,\langle v\rangle$. Hence, from Eqs. (4) and (5), the fractional change in frequency shift due to a fractional change in adsorption time by the influence of the temperature can be written as,[14]

$$\frac{d\Delta\nu}{\Delta\nu} = -\frac{E_a}{k_B.T}\frac{dT}{T}. \tag{6}$$

The temperature coefficient of the cell volume, $TC_v = d\Delta\nu/dT$ (slope in Fig. 9(a)), thus allows to extract the average adsorption energy of Rb on the coating as, $E_a = 0.036$ eV. This value is in close agreement with previously reported studies.[14,33] Part of $TC_v$ might be due to the spin-exchange effect, but as there are no Rb droplets acting as reservoir in the cell volume, one can neglect the influence of this effect. On the other hand, the effect of spin-exchange due to the stem is 10-times smaller in comparison with $TC_v$ (see below).

A similar shift of the clock frequency due to the stem temperature is measured to be $TC_s = 0.22(3)$ Hz/K $\approx 3.2 \times 10^{-11}/K$ as shown in Fig. 9(b). Because the cell stem contains the reservoir of liquid Rb, we mainly attribute this shift to the influence of the atomic density and the related spin-exchange effect, see Refs. 14, 35, 36, and references therein. The shift on the clock frequency due to spin-exchange can be calculated according to Micalizio *et al.*[36] by,

$$\Delta\nu_{se} = -\frac{1}{4}n\bar{v}\lambda_{se}\Delta, \tag{7}$$

where $n$ is the atomic density, $\bar{v} = \sqrt{8k_BT/\pi\mu}$ is the average relative velocity of the colliding atoms at temperature $T$, with $k_B$ the Boltzmann constant and $\mu$ the reduced mass of the colliding particles. $\lambda_{se}$ is the frequency-shift related collisional cross-section, and $\Delta$ is the population difference between the two hyperfine clock levels. The value and sign of $\Delta\nu_{se}$ thus depends on the optical pumping condition in which the atomic sample is prepared for clock operation.

#### 1. Influence on clock instability

From measured variations in the cell's temperature ($\sigma_T = 10$ mK at $10^4$ s), the clock instability due to the temperature coefficient of the cell-volume is estimated as $\sigma_{TC}^{volume} = 2 \times 10^{-12}$, and the contribution on the clock frequency instability due to stem temperature coefficient is $\sigma_{TC}^{stem} = 3.2 \times 10^{-13}$. The limit due to the TC of the cell-volume is thus the dominating one for the clock instability, with the stem's TC being one order of magnitude smaller. The influences of physical parameters on the clock instability in medium to long-term time scales are summarized in Table I.

## V. CLOCK STABILITY

### A. Short-term noise budget

The short-term stability (1 to 100 s) of a passive rubidium frequency standard can be predicted[37] by,

$$\sigma_y = \frac{N_{psd}}{\sqrt{2}.D.\nu_{Rb}}.\tau^{-1/2}, \tag{8}$$

where $N_{psd}$ is the detection noise power-spectral-density when microwave and pump laser are switched on (in closed clock loop). $D$ is the discriminator slope in the error signal close to the line centre, and can be approximated as the ratio of the signal amplitude to the linewidth of DR signal.

The typical measured parameters, estimated signal-to-noise (S/N) limit and shot-noise limit are presented in Table II. Measured noise density, $N_{psd}$ includes the contribution of PM-to-AM (phase modulation to amplitude modulation) noise conversion in the clock cell.[38,39] Using Eq. (8), the S/N limited short-term stability is calculated as $1.3 \times 10^{-12}\,\tau^{-1/2}$.

TABLE II. Noise budget and estimation of signal-to-noise and shot-noise limits.

| Parameter | Value |
|---|---|
| FWHM | 642 Hz |
| Contrast | 11.3% |
| Discriminator, $D$ | 0.41 nA/Hz |
| $N_{psd}$ | 5.1 pA/$\sqrt{\text{Hz}}$ |
| S/N limit | $1.3 \times 10^{-12}\tau^{-1/2}$ |
| Shot-noise limit | $3.3 \times 10^{-13}\tau^{-1/2}$ |

TABLE III. Intensity and frequency light-shift contribution to the clock's short-term instability.

| Physical effect | Coefficient | Parameter variation at $10^4$ s | Formula | Instability ($\tau^{-1/2}$) |
|---|---|---|---|---|
| Intensity<br>Light shift, $\lvert\alpha\rvert$ | 23(3) mHz cm$^2$/$\mu$W | Laser RIN:<br>$2\times10^{-14}$ Hz$^{-1}$ at 300 Hz | $\frac{\sqrt{RIN}.I_L.\alpha}{\nu_{Rb}}$ | $1.2\times10^{-15}$ |
| Frequency<br>Light shift, $\lvert\beta\rvert$ | 413.8(4) mHz/MHz | Laser frequency instability:<br>$\sigma_{LF}=4\times10^{-12}$ (1 − 100 s) | $\frac{\beta.\sigma_{LF}.\nu_L}{\nu_{Rb}}$ | $9.3\times10^{-14}$ |
| Total LS contribution | | $\sigma_{LS}$ | | $9.4\times10^{-14}$ |

The shot-noise limit of the clock occurring due to the statistical nature of the photons is calculated using the noise spectral density, $N_{shot}=\sqrt{2.e.I_{dc}}$, where $e$ is the charge of an electron and $I_{dc}$ is the photocurrent of the DR signal at FWHM.

An additional limit occurs from the LO phase-noise due to the intermodulation effects.[40] A phase-noise measurement of the LO was performed by comparing it with another microwave synthesizer at 6.835 GHz carrier frequency. A flicker level of −77 dBrad$^2$/Hz (at 10 Hz Fourier frequency) and a noise floor of −102 dBrad$^2$/Hz were measured. The phase-noise limited short-term stability, $\sigma_y(\tau)_{PMnoise}$ in a quasi-static model for the square wave modulation with frequency $f_m$ can be written in terms of spectral density,[41] $S_\phi(f_m)$ as

$$\sigma_y(\tau)_{PMnoise}=\sqrt{\sum_{n=1}^{\infty}C_{2n}^2.S_\phi(2nf_m).\tau^{-1/2}}, \tag{9}$$

where

$$C_{2n}=\frac{2n}{(2n-1)(2n+1)}\frac{f_m}{\nu_{Rb}}. \tag{10}$$

By using the clock loop modulation frequency, $f_m=193$ Hz, and considering its even harmonics up to 100 kHz, we estimate the LO phase-noise contribution on clock's short-term stability, $\sigma_y(\tau)_{PMnoise}=6\times10^{-13}\,\tau^{-1/2}$.

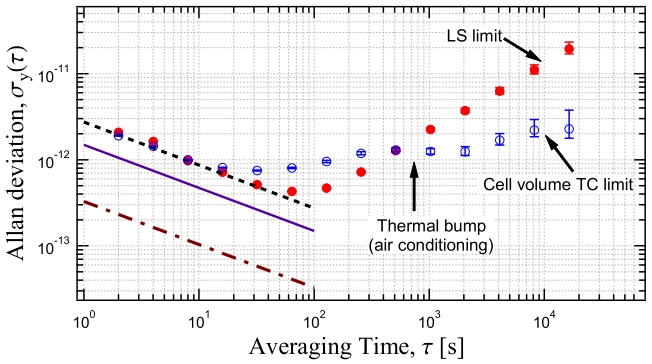


FIG. 10. Measured clock stability using the wall-coated Rb cell. Closed circles show clock stability data without intensity LS compensation; open circles denote the clock stability with intensity LS compensation by the detuning method. The dotted line represents the measured clock short-term stability of $2.75\times10^{-12}\tau^{-1/2}$, the solid line indicates the estimated total limit (Eq. (11)), and dashed-dotted line shows the shot-noise limit of $3.3\times10^{-13}\tau^{-1/2}$.

The intensity and frequency light-shifts also influence the short-term stability of the clock, via the laser's relative intensity noise (RIN) and laser frequency instability, which perturb the clock transition on short-time scales. Table III summarizes these effects and resulting limits on the short-term clock stability.

Eventually, the overall short-term clock stability can be estimated from the sum of the squares of the individual limits by the following equation as $1.5\times10^{-12}\tau^{-1/2}$:

$$\sigma_y(\tau)=\sqrt{\sigma_{S/N}^2+\sigma_{PMnoise}^2+\sigma_{LS}^2}. \tag{11}$$

The experimentally measured short-term stability of the DR clock using the paraffin-coated cell is shown in Fig. 10. The measured short-term stability of $2.75\times10^{-12}\tau^{-1/2}$ is in reasonable agreement with the estimated stability of $\simeq1.5\times10^{-12}\tau^{-1/2}$. The clock run without laser detuning (closed circles) shows its medium-to long-term stability limited at $1.8\times10^{-11}$ due to intensity light-shift as predicted (see Table I). In the second run (open circles), the reduction of the intensity light-shift by a factor of 40 was implemented using the AOM. Here, the clock stability is limited to around $2\times10^{-12}$ at $10^4$ s by the temperature coefficient of the coating material. This limitation is an intrinsic property of the coating material and hence gives the ultimate limit for this particular clock, unless improvements on the temperature control of the cell are implemented. A linear drift of $8.5\times10^{-12}$/day was measured, including also the ageing of the coating material. Presently, we have not studied further this drift.

## VI. CONCLUSIONS AND PROSPECTS

Investigations on the paraffin coating material characteristics were performed by measuring the $T_1$ and $T_2$ relaxation times for a wall-coated Rb cell, and show that a polarized Rb atom undergoes about 2255 wall collisions (at 300 K) before losing its polarized state. The optical-microwave double-resonance spectroscopic studies with a paraffin coated cell inside a $TE_{011}$ magnetron cavity showed a narrow linewidth of <650 Hz with a large signal contrast >11%. Systematic studies of the parameters that influence the medium to long-term stability—notably by the perturbations due to intensity and frequency light-shifts, microwave power shift and shifts on clock transition due to temperature variations that occurs due to the atom-wall interactions—were quantified and their instability contributions on the clock were estimated.

We showed that wall-coated cells can be used for realization of high-performance Rb clocks even when using small cells (1.4 $cm^3$ volume) in view of compact clocks. Measured clock stabilities are in agreement with the calculated limits on both the short-term and medium-term timescales. Using detuning of the laser frequency, the limitation to medium-term clock stability arising from the intensity light-shift was suppressed, which results in the clock stability being limited by the temperature coefficient of the coating. This temperature coefficient can in principle be compensated by adding a small amount of a suitable buffer-gas to the cell. This possibility was discussed previously[30,42] for linewidth studies, but not for compensation of the temperature coefficient of the coating.

Use of wall-coatings also is of high interest to achieve narrow line-widths from cells of smaller dimensions or even microfabricated cells,[43] but better coating materials allowing for a higher number of wall collisions at higher cell temperatures are required. Recent work of Seltzer *et al*.[30] on octadecyltrichlorosilane (OTS) shows that the coating can sustain higher temperatures up to 170 °C. Surface science techniques help to characterize the quality of the coating materials to the precision of monolayers.[44,45] However, the influence of this coating's temperature coefficient on the clock transition is not yet known and may be expected to have an important impact on the achievable clock stability.

## ACKNOWLEDGMENTS

We acknowledge financial support from the European Space Agency (ESA), Swiss National Science Foundation (SNSF) and Swiss Space Office (SSO). We thank our colleagues F. Gruet, P. Scherler, and M. Durrenberger for technical support, M. Pellaton for useful discussions, and C. E. Calosso (INRIM, IT) for helpful exchanges on microwave synthesizers. We also thank S. Knappe (NIST, USA) for fruitful discussions on $T_1$ and $T_2$ relaxation measurements.

[1]J. Camparo, Phys. Today **60**(11), 33 (2007).
[2]R. H. Dicke, Phys. Rev. **89**, 472 (1953).
[3]R. H. Romer and R. H. Dicke, Phys. Rev. **99**, 532 (1955).
[4]H. G. Robinson, E. S. Ensberg, and H. G. Dehmelt, Bull. Am. Phys. Soc. **3**, 9 (1958).
[5]H. G. Robinson and C. E. Johnson, Appl. Phys. Lett. **40**, 771 (1982).
[6]H. G. Robinson and C. E. Johnson, IEEE Trans. Instrum. Meas. **IM-32**, 1 (1983).
[7]M. A. Bouchiat and J. Brossel, Phys. Rev. **147**, 41 (1966) and references therein.
[8]W. Franzen, Phys. Rev. **115**, 850 (1959).
[9]V. Liberman and R. J. Knize, Phys. Rev. **34**, 5115 (1986).
[10]M. T. Graf *et al*. Phys. Rev. A **72**, 023401 (2005).
[11]M. V. Balabas, D. Budker, J. Kitching, P. D. D. Schwindt, and J. E. Stalnaker, J. Opt. Soc. Am. B. **23**, 1001 (2006).
[12]V. Shah, S. Knappe, P. D. D. Schwindt, and J. Kitching, Nature Photon. **1**, 649 (2007).
[13]M. V. Balabas, T. Karaulanov, M. P. Ledbetter, and D. Budker, Phys. Rev. Lett. **105**, 070801 (2010).
[14]D. Budker, L. Hollberg, D. F. Kimball, J. Kitching, S. Pustelny, and V. V. Yashchuk, Phys. Rev. A **71**, 012903 (2005).
[15]R. P. Frueholz, C. H. Volk, and J. C. Camparo, J. Appl. Phys. **54**, 5613 (1983).
[16]G. Singh, P. Dilavore, and C. O. Alley, Rev. Sci. Instrum. **43**, 1388 (1972).
[17]C. Szekely and R. Drullinger, Proc. SPIE **1837**, 299 (1992).
[18]E. Breschi, G. Kazakov, C. Schori, G. Di Domenico, G. Mileti, A. Litvinov, and B. Matisov, Phys. Rev. A **82**, 063810 (2010).
[19]S. Bize, Y. Sortais, M. S. Santos, C. Mandache, A. Clairon, and C. Salomon, Europhys. Lett. **45**, 558 (1999).
[20]B. S. Mathur, H. Tang, and W. Happer, Phys. Rev. **171**, 11 (1968).
[21]C. Affolderbach, F. Droz, and G. Mileti, IEEE Trans. Instrum. Meas. **55**, 429 (2006).
[22]G. Mileti, I. Ruedi, and H. Schweda, in *Proceedings of 6th European Frequency and Time Forum* (The European Space Agency Publications Division, ESA SP-340, 1992), p. 515.
[23]A. Risley, S. Jarvis, and J. Vanier, J. Appl. Phys. **51**, 4571 (1980).
[24]J. Vanier, R. Kunski, A. Brisson, and P. Paulin, J. Phys. **12**, 139 (1981).
[25]M. V. Balabas, M. I. Karuzin, and A. S. Pazgalev, JETP Lett. **70**, 3 (1999).
[26]M. Stephens, R. Rhodes, and C. Wieman, J. Appl. Phys. **76**, 3479 (1994).
[27]J. Vanier and C. Audoin, *The Quantum Physics of Atomic Frequency Standards* (Adam Hilger, Bristol 1989).
[28]M. V. Balabas, K. Jensen, W. Wasilewski, H. Krauter, L. S. Madsen, J. H. Miller, T. Fernholz, and E. S. Polzik, Opt. Express **18**, 5825 (2010).
[29]C. Affolderbach and G. Mileti, Rev. Sci. Instrum. **76**, 073108 (2005).
[30]S. J. Seltzer and M. V. Romalis, J. Appl. Phys. **106**, 114905 (2009).
[31]S. Micalizio, A. Godone, F. Levi, and C. Calosso, Phys. Rev. A **79**, 013403 (2009).
[32]C. Affolderbach, C. Andreeva, S. Cartaleva, T. Karaulanov, G. Mileti, and D. Slavov, Appl. Phys. B **80**, 841 (2005).
[33]C. Rahman and H. G. Robinson, IEEE J. Quantum Electron. **23**, 452 (1987).
[34]H. M. Goldenberg, D. Kleppner, and N. F. Ramsey, Phys. Rev. **123**, 530 (1961).
[35]W. Happer, Rev. Mod. Phys. **44**, 169 (1972).
[36]S. Micalizio, A. Godone, F. Levi, and J. Vanier, Phys. Rev. A **73**, 033414 (2006).
[37]T. Bandi, C. Affolderbach, C. E. Calosso, and G. Mileti, Electron. Lett. **47**, 698 (2011).
[38]G. Mileti, J. Deng, F. L. Walls, D. A. Jennings, and R. E. Drullinger, IEEE J. Quantum Electron. **34**, 233 (1998).
[39]J. G. Coffer, M. Anderson, and J. C. Camparo, Phys. Rev. A **65**, 033807 (2002).
[40]G. J. Dick, J. D. Prestage, C. A. Greenhall, and L. Maleki, in *Proceedings of the 22nd Precise Time and Time Interval meeting* (PTTI), Vienna, VA (NASA conference publication, 3116, 1990), pp. 487–508.
[41]J. Q. Deng, G. Mileti, R. E. Drullinger, D. A. Jennings, and F. L. Walls, Phys. Rev. A **59**, 773 (1999).
[42]S. Knappe and H. G. Robinson, New J. Phys. **12**, 065021 (2010).
[43]S. Knappe, P. D. D. Schwindt, V. Gerginov, V. Shah, L. Liew, J. Moreland, H. G. Robinson, L. Hollberg, and J. Kitching, J. Opt. A, Pure Appl. Opt. **8**, S318 (2006).
[44]Y. W. Yi, H. G. Robinson, S. Knappe, J. E. Maclennan, C. D. Jones, C. Zhu, N. A. Clark, and J. Kitching, J Appl. Phys. **104**, 023534 (2008).
[45]S. J. Seltzer *et al*. J. Chem. Phys. **133**, 144703 (2010).